The UNAV, a Wind-Powered UAV for Ocean Monitoring: Performance, Control and Validation

The UNAv, a wind-powered UAV for ocean monitoring: performance, control and validation

Gabriel D. Bousquet, Michael S. Triantafyllou, Jean-Jacques E. Slotine

***Abstract*— Wind power is the source of propulsive energy for sailboats and albatrosses. We present the UNAv, an Unmanned Nautical Air-water vehicle, that borrows features from both. It is composed of a glider-type airframe fitted with a vertical wing-sail extending above the center of mass of the system and a vertical surface-piercing hydrofoil keel extending below. The sail and keel are both actuated in pitch about their span-wise axes. Like an albatross, the UNAv is fully streamlined, high lift-to-drag ratio and generates the gravity-cancelling force by means of its airborne wings. Like a sailboat, the UNAv interacts with water and may access the full magnitude of the wind. A trim analysis predicts that a 3.4-meter span, 3 kg system could stay airborne in winds as low as 2.8 m/s (5.5 knots), and travel several times faster than the wind speed. Trim flight requires the ability to fly at extreme low height with the keel immersed in water. For that purpose, a multi-input longitudinal flight controller that leverages fast flap actuation is presented. The flight maneuver is demonstrated experimentally.**

I. Introduction

Increasing the endurance and range of unmanned aerial vehicles (UAVs) is an important challenge. In some applications, improved endurance would allow to reduce mission costs and increase mission performance. In others, current limitations prevent the use of UAVs altogether. Blue-ocean monitoring is one instance where endurance limitations prevent penetration of UAVs technologies. In effect, the oceans, covering 70% of the Earth remain acutely under-monitored, despite the fact that offshore observations performed by long-range surface and airborne craft would benefit many industries and scientific fields.

A striking illustration, the Southern Ocean accounts for about 40% of the oceanic uptake of anthropogenic CO_2 [1]. Being removed from major commercial shipping routes, under frequent cloud cover, and subject to strong winds and storms, this large sink of carbon is significantly less observed or sampled than other oceans which play a smaller role as carbon sinks but are more straightforward to monitor. Swarms of long-range UAVs could help fill that crucial knowledge gap.

UAVs that carry their propulsive fuel have a limited endurance ranging from a few hours (battery) to a few days (gas) [2]. Breaking this endurance barrier would require higher density energy storage, in-flight refueling [3], or energy extraction from the environment. On land, solar power could help extend the endurance of small-scale, electric, fixed-wing UAVs from a few hours to full day operation [4]. However, solar-powered multi-day endurance is a fundamentally hard challenge. In particular, it requires small wing loadings, *i.e.* is seriously payload limited [5] or requires very large systems [2].

Over water, reliable winds and waves constitute additional sources of usable energy. Long-range, small-scale ($\sim$1–3 m) autonomous surface vehicles that rely on wave or wind power for propulsion have been developed [6], [7], [8]. Wave gliders converts the up-and-down motion of waves into forward motion by means of underwater "flapping wings". Wind-powered surface craft (sailboats), extract energy from the wind by transferring momentum from a fast medium (the windy air) by means of a sail, to a slow medium, (the water), by means of a keel. The overall reduction of the velocity mismatch between the two media is a sign of energy extraction.

In general, these small-scale surface craft are very slow $\lesssim 2.5$ m/s due to the large drag of their hulls (lift-to-drag ratio of order unity) and their dynamic response to waves. Hydrofoils sailboats lift their hull out of the water by means of underwater, high lift-to-drag ratio hydrofoil wings and may travel several times faster than traditional sailboats. However, to remain efficient, hydrofoil sailboats need to precisely follow the water surface in order to neither wet their hull nor breach the water with their hydrofoils. This makes the design and operation of small-scale hydrofoil craft challenging. Overall, small-scale autonomous sailboats may be efficient at harnessing wind energy, but they dissipate it through their large drag.

The wandering albatross (*Diomedea Exulans*), is the size of a small drone at a typical 10 kg and 3 m span. Mostly found in the southern oceans between 30° and 60° S, where strong winds prevail, albatrosses fly by extracting their propulsive energy from the wind through a specific flight technique called dynamic soaring [9]. They typically travel 500 miles per day [10]. Dynamic soaring can be thought of as sequential sailing: the albatross cyclically transfers momentum from the fast wind in altitude $z \sim 10$ m to the slower boundary layer near the surface $z \sim 1$ m, acting in turn as a sail in the wind and as a keel in the boundary layer. With a glide ratio approaching 20, albatrosses are high-performance, low-drag systems. However, unlike sailboats, they only harness a small fraction of the wind magnitude, because the boundary layer is typically only somewhat ($\sim 25\%$) slower than the wind in altitude.

Overall, an efficient wind power system would merge the respective assets of sailboats and albatrosses, by following

Department of Mechanical Engineering, Massachusetts Institute of Technology, Cambridge, MA 02139, USA; {g_b,mistetri,jjs}@mit.edu

This work was partially funded by a Link Ocean Engineering and Instrumentation fellowship.

the two general guidelines: 1) transfer momentum from the wind to the water like sailboats ($\sim$4x factor improvement compared to albatrosses), and 2) be fully streamlined and only interact with the water for the purpose of wind-water momentum transfer by means of a streamlined "keel" appendage (with a potential order-of-magnitude improvement in lift-to-drag ratio compared to sailboats).

In this study we present the UNAv, a wind-powered Unmanned Nautical Air-water vehicle that follows the aforementioned design guidelines by merging the wings of albatrosses and the sail and keel of sailboats. We analyze the UNAv performance in trim flight with a static aero-hydrodynamic model. Trim flight requires the ability to fly and maintain the system at extreme low heights while a keel is immersed in the water generating a side lift force. We design the controllers for a test platform. In particular, we build a multi-input longitudinal controller for precise height control inspired by feedback linearization and eigenvector placement techniques. It takes advantage of the high-bandwidth of the flap actuation on off-the-shelf RC airplanes for fast disturbance rejection. Finally, a flight test experimentally demonstrates the feasibility of the maneuver.

II. UNAv: A HIGH-SPEED, WIND-POWERED, AIR-WATER SYSTEM FOR OCEAN MONITORING

The conceptual vehicle considered in this study is displayed in figure 1. Its central component is the main airframe (red). The system is designed to skim above the water surface as a low-height airplane or glider. As with sailboats, propulsion is performed by a pair of appendages: a vertical wing sail (green) and a vertical, surface piercing keel (blue tip of the lower appendage). When the UNAv is flying in the presence of wind, it may individually control the lift force of the sail and the keel by actuating their respective pitch angles θ_s, θ_k. The lift forces of the sail and keel are orthogonal to the local fluid flow. In the presence of wind $\mathbf{W}$, the local air-relative velocity $\mathbf{V}$ and the local water-relative (or "ground") velocity $\mathbf{U}$ are different. As a result, the sail and keel lifts may be misaligned and their sum force may generate a net thrust. For instance, in figure 1a, the airframe is aligned with the local air flow. The keel sail force is sideways (towards $-\mathbf{x}_b$) while the keel force has both a sideways and a forward (thrust) component. With the right amount of lift, the lateral components of the forces cancel each other, resulting in an overall thrust. If the sail and keel lift forces are large enough, they may overcome the total drag of the system. Note that because water is 800 times denser than air, the active part of the keel (in blue) is much smaller than the sail. Ideally, the 40-cm-long beam (white) supporting at its tip the active part of the keel is out of the water and does not generate any hydrodynamic force.

For large lift-to-drag ratios, it can be shown with simple trigonometry on figure 1a that a good approximation for the travel speed of the system in crosswind flight is $U = (\text{sail lift})/(\text{total drag})W$, such that high-performance systems may travel at several times the wind speed, as described in the trim analysis below.

Note that this system is fundamentally different from hydrofoil sailboats with underwater wings, as weight is cancelled with airborne lifting surface. Unlike hydrofoil sailboats, the UNAv only needs to have the keel immersed on average and may leave the water surface—for instance in order to avoid waves.

In this study we consider a 3 kg system based on the planform of the Supra, a glider airframe designed by Mark Drela, with the main wing dihedral removed. The airframe is 3.4 meters in span b_a with an aspect ratio of 17 (reference chord and wing area $c_a = 19$ cm and $S = 0.67$ m^2). The airframe geometry is publicly available within the source code of the GPL software AVL, utilized below [11]. The sail considered in this study is based on the wing planform of the Supra, with the chord and span scaled by a factor 5/3 and 3/5 respectively, to $c_{s,\max} = 40$ cm and $b_s = 1$ m, respectively (reference sail area $S_s = 0.33$ m^2). The selected wing sail profile is a NACA 0009. The active part of the keel is assumed rectangular, with a chord $c_h = 2$ cm and an immersed span $h = 10$ cm. The selected keel profile is a NACA0014 such that the keel is 2.8 mm thick. The distance between the center of gravity and the keel's tip is $b_h = 50$ cm. The system is designed to fly at a height $b_h - h = 40$ cm above the water surface. The sail and keel are actuated along their quarter-chords, which are located at the vertical of the UNAv's center of gravity.

III. PERFORMANCE ANALYSIS

The goal of this section is to quantitatively assess the potential for wind-powered propulsion of a perfectly controlled UNAv in trim state. For that purpose, we build a model that is high-fidelity in terms of aerodynamic performance, but as much as possible simplified in terms of dynamics.

A. Trim analysis

We assume that the UNAv is flying in a constant wind field above a flat water surface, and that by appropriate control action (rudder-aileron-elevator) it is able remain at its design height, maintain zero roll, and with no air-relative sideslip, as illustrated in figure 1a.

The aerodynamic forces and moments of the sail and airframe are computed separately. Below, we discuss the modeling of the aero- and hydrodynamic forces and moments generated by the three components of the UNAv, when flying with no air-relative sideslip.

1) Airframe Aerodynamics (no sail): An AVL model of the airframe *without the sail* is defined. The profile drag of the airfoils is modeled within AVL by fitting the drag polar of the respective airfoils at a Reynolds number of 200k computed with Xfoil [12]. The lift force takes the form $\mathbf{L}_\text{a} = {}^1\!/_2 C_L \rho S V^2 \mathbf{z}$. All quantities of interest are computed with AVL assuming trim and a set height above water (modeled as a plane of symmetry 40 cm below the airframe) to account for ground effect. In particular the drag force is expressed as $\mathbf{D}_\text{a} = -{}^1\!/_2 (C_{D,0} + \delta C_D(C_L)) \rho S V^2 \mathbf{x}_b$, where $C_{D,0} = 0.015$ is the drag coefficient at no lift due to the fuselage and

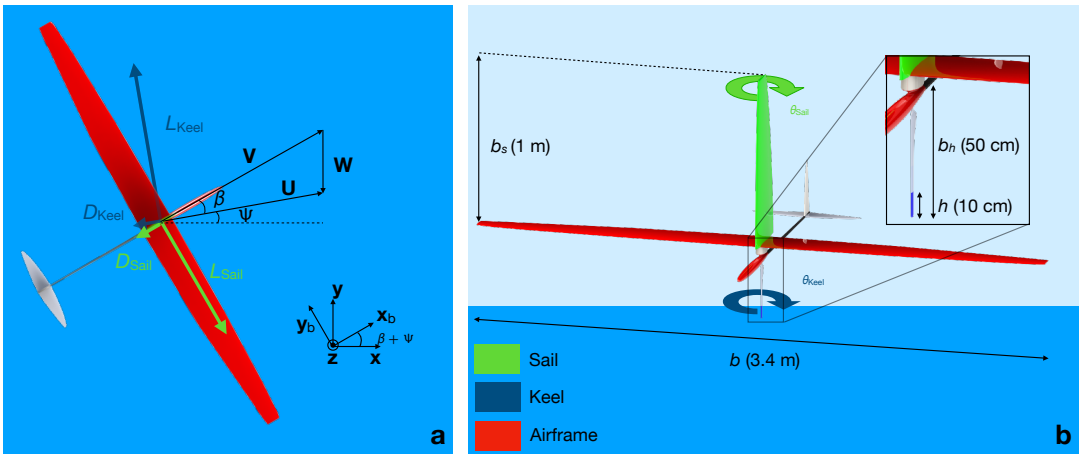

Fig. 1: The UNAv, a wind-powered Unmanned Nautical Air-water vehicle.

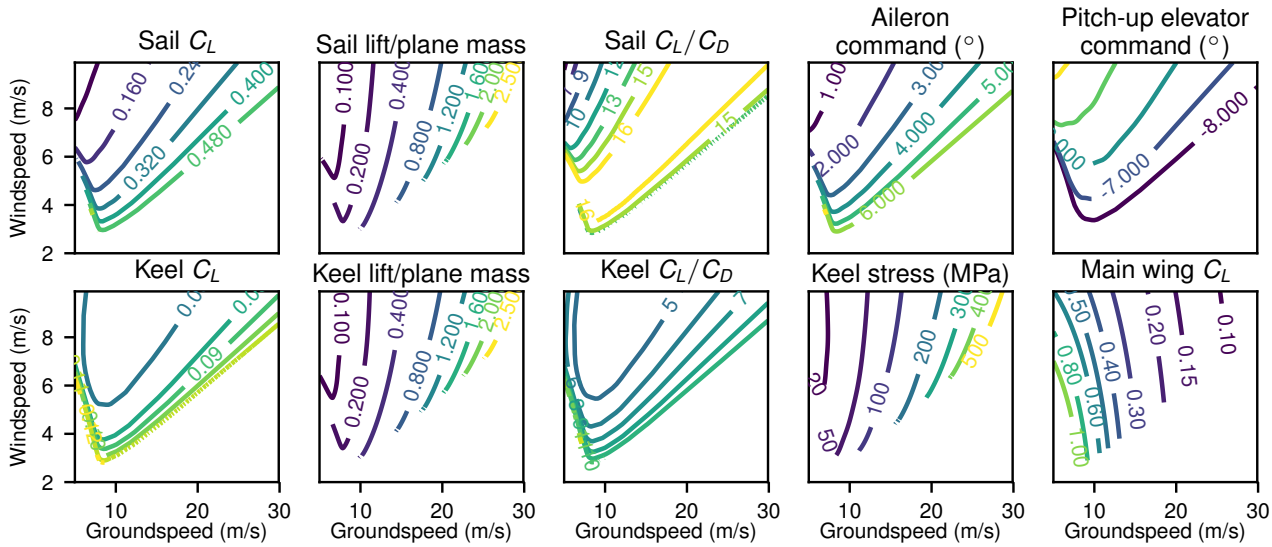

Fig. 2: Trim conditions for a 3kg, 3.4m span UNAv in crosswind travel.

parasitic drag. With this value for $C_{D,0}$, the maximum lift-to-drag ratio in the absence of ground effect would be 20. The function $\delta C_D(C_L)$ is the drag coefficient of the airframe lifting surfaces, computed with AVL. The maximum lift-to-drag ratio in ground effect is 23.5. AVL also computes the elevator input required to generate the set lift force $\delta_e(C_L)$ and maintain trim in pitch, as well as the control authority in pitch $C_{m_{\delta_e}}$ and in roll $C_{l_{\delta_a}}$ due to elevator and aileron inputs. Specifically, the change in pitching moment due an elevator input is $\delta M_y(\delta_e) = {}^1\!/\!_2\rho S c_a C_{m_{\delta_e}} \delta_e V^2$ and the change in rolling moment due to aileron input is $\delta M_x(\delta_a) = {}^1\!/\!_2\rho S b_a C_{l_{\delta_a}} \delta_a V^2$ [13].

2) Sail Aerodynamics: An AVL model of the airframe *with the sail included* is defined. The profile drag for each section is based on the polar of the NACA 0009 at a Reynolds number of 200k computed with Xfoil. Within the no-sideslip hypothesis, a side lift force $\mathbf{L}_s = -{}^1\!/\!_2 C_{L,s}\rho S_s V^2 \mathbf{y}_b$ is generated by pitching the sail along the z axis. There is an additional drag term due to the sail $\mathbf{D}_s = -{}^1\!/\!_2(C_{D,0,s} + \delta C_{D,s})\rho S_s V^2 \mathbf{x}_b$, and a pitching moment due to drag $M_{y,s} = {}^1\!/\!_2\rho S_s b_s C_{m,s}(C_{L,s})V^2$ which are approximately decoupled from the drag due to vertical lift on the main airframe. The rolling moment due to the sail lift is $M_{x,s} = {}^1\!/\!_2\rho S_s b_s \frac{dC_l}{dC_{L,s}} C_{L,s} V^2$. All aerodynamic coefficients are computed with AVL.

3) Hydrodynamic forces on the keel: As for the sail, the drag $\mathbf{D}_k$, pitching and rolling moments $\tau, M_{x,k}$ are computed with AVL as a function of the keel lift $\mathbf{L}_k$. The lift and drag forces are perpendicular and parallel to the local flow which is $-\mathbf{U}$. For Froude numbers $U/\sqrt{gc_h}$ above unity, the boundary condition at the air-water interface is a plan of anti-symmetry [14], which AVL can model. Here the Froude number is above 15, within the domain of validity of the approximation.

AVL does not model cavitation (in zones of low pressure the water may boil and gas bubbles appear, perturbing the flow. Cavitation occurs at large speeds $U > 20$ m/s) or ventilation (air from the atmosphere is entrained to zones

of low pressure, breaching the water surface. Ventilation is a complex phenomenon which is favored at large angle of attack, beyond stall, and high speed) [15]. As illustrated in figure 2, the flying sailboat may operate in conditions where neither cavitation nor ventilation are likely to occur. Note that there is also a small drag term due to spray making [16].

The active part of the keel is subject to large forces $\sim$10N relative to its size. Assuming that the beam supporting the active part of the keel needs to remain slender for an extra length h above the water surface (as it is prone to frequent immersion, in which case its hydrodynamic properties are important), and that above that it is less likely to be immersed and can therefore be thicker, the maximum stress experienced by the keel is estimated with a beam model of length $2h$ uniformly loaded on its outer half.

4) Static equations: When the system is traveling in the trim (static) state, the following equations hold:

$$\begin{aligned} F_x &= 0 = L_\mathrm{k}\sin\beta - D_\mathrm{k}\cos\beta - D_\mathrm{s} - D_\mathrm{a} \\ F_y &= 0 = L_\mathrm{k}\cos\beta + D_\mathrm{k}\sin\beta - L_s \\ F_z &= 0 = L_\mathrm{a} - mg \\ M_x &= 0 = M_{x,k} + M_{x,s} + \delta M_x(\delta_a) \\ M_y &= 0 = \tau + M_{y,s} + \delta M_y(\delta_e) \\ M_z &= 0 \quad \text{rudder-controlled no-sideslip assumption} \end{aligned} \tag{1}$$

The trim state can now be computed by solving equation (1).

B. Performance

The trim state is computed in crosswind flight $\Psi = 0$, for various values of the wind speed and travel speed. Flight quantities are collected in figure 2. Overall, within the model, feasible trim states exist for wind speeds as low as 2.8 m/s (5.5 kts). For wind speeds higher than 4 m/s the maximum reachable ground speed scales approximately linearly with wind speed as $U = 3.5W$.

a) Minimum wind: The minimum-wind point of operation in crosswind has a travel speed of 8.4 m/s (three times the wind speed), with the sail and keel each producing a lift force of 20–30% that of the main wing. The lift coefficient of the sail is 0.6 while the lift coefficient of the keel is 0.13 with a lift-to-drag ratio of 11 (indicating that from an efficiency standpoint, the keel is hydrodynamically oversized). The aileron and elevator commands required for maintaining the horizontal attitude are 7° and 11°, respectively. The elevator is compensating a general pitch-up tendency due the sail drag and the keel lift, which is tilted towards positive $\mathbf{x}_\mathrm{b}$ (see figure 1a). The maximum load stress experienced at the root of the keel is 64 MPa, well below the fatigue strength of Aluminum, stainless steel or carbon fiber composites.

The polars of figure 3 collect the minimum wind required for sustained flight as a function of the direction of travel Ψ. Within the model, travel is possible going upwind by 45° in a 3.5 m/s wind, and nearly 45° downwind in 4.5 m/s wind. Perhaps counter-intuitively, the model predicts that less wind is required to travel slightly upwind than exactly crosswind. This is likely due to the fact that upwind travel is associated with a higher apparent wind seen by the airframe, which translates to a smaller induced drag.

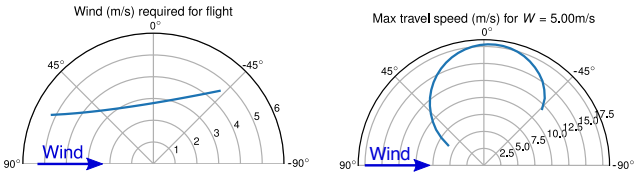

Fig. 3: Left: Minimum wind required for flight as a function of the cross-country heading Ψ for a 3.4 m span, 3 kg UNAv in trim condition. The 0° direction represents crosswind travel. Right: Maximum travel speed as a function of the cross-country heading in a 5m/s wind.

b) Maximum travel speed: In high winds $W \gtrsim 4$ m/s, the model predicts a linear relationship between wind speed and maximum reachable speed $U_\mathrm{max}(\Psi, W)$. The maximum speed is then reached for a sensibly constant set of sail and keel lift coefficients (in crosswind, 0.5 and 0.11). At high travel speeds the stress on the keel due to lift scales quadratically and quickly surpasses the strength of stainless steel or carbon fiber composite beyond speeds of 25–30 m/s. Furthermore, at such high speeds cavitation may occur, further reducing the reliability of the present model. Taking these additional constraints into account, the maximum travel speed should in fact plateau in high winds. The polar of figure 3 shows the system's ground speed as a function of the travel direction Ψ in the case $W = 5$ m/s. The maximum ground speed is reached for an overall travel direction 5° down from crosswind. For $\Psi = \pm 40°$, the speed is still over 65% of the maximum speed.

c) Comparison with albatrosses and sailboats: The trim study suggests that the flying sailboat could stay aloft in winds as low as 2.8 m/s, about a third of the wind required for albatrosses to perform dynamic soaring [9], [17] (a difference not explained by differences in wing loading alone). Furthermore, computer simulations suggest that upwind dynamic soaring is hardly feasible [17], consistent with the high energy expenditure of albatrosses traveling upwind [18]. In contrast, the model predicts that flying sailboat may travel within $\pm 40°$ of crosswind both down- and upwind. This is accomplished at speeds several times faster than traditional sailboats, with the added capability to take off from the water surface vicinity, either for obstacle avoidance, or for monitoring purposes.

C. An operational challenge: keel size and force

As mentioned above, in all trim states considered in figure 2, the lift coefficient of the 2×10 cm hydrofoil is extremely low $C_L \lesssim 0.15$. For pure hydrodynamic efficiency, one would typically wish the lifting surface to operate at its maximum lift-to-drag ratio $C_L/C_D \gtrsim 0.5$.

Intuitively, the lift of the keel is approximately equal to that of the sail, which size must typically be smaller than the wings for its roll moment to be balanced by aileron inputs. If the keel and sail were operating at the same lift coefficient,

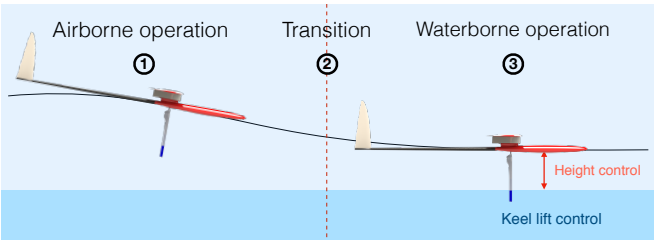

Fig. 4: Critical maneuver for the UNAv: extreme low height flight, keel immersion and force generation.

the keel should be 800 times smaller than the sail (the density ratio between air and water), *i.e.* less than about 5 cm^2 for the airframe considered.

Conversely, immersion of a smaller keel with the same relative accuracy in depth requires more precise longitudinal control, and may constitute a challenge altogether in the presence of waves. Other issues such as structural strength and wave clearance may also be more acute for small keels.

Accordingly, there is a tradeoff in keel size, with the system presented in this study being oversized by a factor $\sim 3-4$ compared to optimal hydrodynamic efficiency alone. While a large keel simplifies the longitudinal control problem, it complicates the attitude control problem because at high C_L the keel is potentially able to generate moments too large to be compensated by the airframe's aileron or elevator control authority.

Even with an oversized keel, the static model predicts a 3-fold improvement in terms of minimum required wind compared to purely dynamic soaring systems, a vastly improved upwind-ability, and a $\geq$ 3-fold improvement in travel speed compared to sailboats. In the next sections we show experimentally that with active control of the keel pitch θ_{k} it is possible to generate the desired lift with the keel of a system sized as above, while at the same time controlling the height and attitude of the UNAv with the control surfaces of the airframe.

IV. Critical maneuver

Reaching and maintaining the trim state described in section III-A requires performing the following maneuvers: 1) fly at low height with high precision and accuracy (a small fraction of the keel's span); 2) transition in a controlled way between phases when the keel is outside of the water and when it is immersed; 3) immerse the keel and generate usable force with it while retaining control of the airframe's attitude. Requirement 2 is necessary to fly in rough seas when the system needs to take off in order to avoid a steep or breaking wave. The maneuvers are the key enablers to operating the system in an energy-positive or energy-neutral trim state where wind is used for propulsion.

Note that the algorithmic control framework needed to perform maneuvers 1 to 3 may be implemented and tested without the physical sail. Accordingly, the overall sequence proposed in figure 4 demonstrates all aforementioned critical control aspects in one single experiment.

Below, we present a set of controllers that were utilized to demonstrate the maneuver on an experimental platform.

V. Control

It is well-known that for a left-right symmetric aircraft in horizontal trim, the longitudinal dynamics (height control) and the lateral dynamics (roll and yaw) are decoupled [13]. For this experiment, four controllers were developed: longitudinal control, roll control, yaw control, and keel control.

A. Longitudinal control

We utilize a longitudinal controller that makes use of the fact that on RC airframes, the flaps and elevators have the same bandwidth. On tailed aircraft, high-speed control of the altitude with the elevator only is complicated by the generation of downwash by the main wing which is convected to the elevator. The flaps on the main wing are comparatively easier to model. Intuitively, the flaps may be used for high-speed but low-amplitude height control and disturbance rejection, while the elevator is used for slow but large amplitude control. Consider the linearized equations of motion for the longitudinal dynamics below [13]. The first equation models the dynamics of the aircraft's height z, positive up, and the second equation corresponds to its pitch angle θ, positive when pitching up:

$$m(\ddot{z}+g)-qSC_L^0+C_{L_\alpha}(\dot{z}/V-\theta) = qSC_{L_{\delta_f}}\delta_f-qS|C_{L_{\delta_e}}|\delta_e, \tag{2a}$$

$$I_{yy}\ddot{\theta}+\frac{qSc^2}{2V}|C_{m_q}|\dot{\theta}+mgd_g\theta+qSc|C_{m_\alpha}|(\theta-\dot{z}/V) = qSc|C_{m_{\delta_e}}|\delta_e+\tau_{\text{keel drag}} \tag{2b}$$

where $q = {}^1\!/_2\rho V^2$ is the flow dynamic pressure, d_g is the distance between the center of gravity and the center of lift, and δ_f and δ_e are elevator and flaps inputs, respectively. The longitudinal dynamics is feedback-linearized into the form

$$\ddot{z} = u_1 \tag{3a}$$

$$\ddot{\theta} = u_2 \tag{3b}$$

with

$$u_1 = C_L Sq/m - g \tag{4a}$$

$$\text{with } C_L = C_L^0 + C_{L_\alpha}(\theta-\dot{z}/V)+C_{L_{\delta_f}}\delta_f \tag{4b}$$

$$u_2 = \frac{1}{I_{yy}}\Big(-\frac{qSc^2}{2V}|C_{m_q}|\dot{\theta}-mgd_g\theta - qSc|C_{m_\alpha}|(\theta-\dot{z}/V)+qSc|C_{m_{\delta_e}}|\delta_e\Big) \tag{4c}$$

such that by height and pitch control are formally decoupled. A tracking controller may then be designed for both z and θ separately. For instance, pole placement with integral control may be performed through the use of *composite variables* [19]. Define the composite variables $\zeta = z+\lambda_{i,z}\int z$ and $\vartheta = \theta+\lambda_{i,\theta}\int\theta$, with error signals $\tilde{\zeta} = \zeta-\zeta_d$ and

$\tilde{\vartheta} = \vartheta - \vartheta_d$ (for instance, ζ_d is defined from the height set-point z_d as $\zeta_d = z_d + \lambda_{i,z} \int z_d$). The integral controllers

$$u_1 = -\lambda_{i,z}\dot{z} + \dddot{\zeta}_d - 2\lambda_z\ddot{\tilde{\zeta}} - \lambda_z^2\dot{\tilde{\zeta}} \tag{5a}$$

$$u_2 = -\lambda_{i,\theta}\dot{\theta} + \ddot{\vartheta}_d - 2\lambda_\theta\dot{\tilde{\vartheta}} - \lambda_\theta^2\tilde{\vartheta} \tag{5b}$$

are such that $(d/dt + \lambda_z)^2\tilde{\zeta} = 0$ which implies $\tilde{z} \to 0$.

In practice, the authority of flap control is small, saturates, and is conducive to additional drag. Therefore it is desirable for slow but large amplitude changes in z to be driven by the elevator through the state θ, and for the flaps to handle the fast dynamics and disturbances but return to $\delta_f = 0$ in steady-state.

This can be accomplished by defining the pitch set-point θ_d with the following slow dynamics $(\frac{1}{\lambda_e}\frac{d}{dt}+1)^2\theta_d = (u_1 + g - C_L^0)/C_{L_\alpha} + \dot{z}/V$. Indeed: 1) With this choice, equation (2) remains stable (contracting [20]) because it is a hierarchy of two stable subsystems, namely subsystem (3a, 5a) which does not depend on θ provided the coefficients are known, and subsystem (3b, 5b) for which z, θ_d are bounded inputs. 2) In steady state, the unique equilibrium $\theta = \theta_d$ brings $\delta_f = 0$ in equation (4b).

Overall, the controller makes use of techniques from feedback linearization and eigenvector placement. It could easily be extended with a nonlinear model of the lift and angles. Note also that it is stable even if V is time-dependent.

B. Roll control

Roll control is comparatively less complex than longitudinal control. This section gives a short description of the controller utilized. Within the roll-subsidence approximation [13], the roll dynamics is

$$I_{xx}\ddot{\phi} + \frac{qSb^2}{V}C_{lp}\dot{\phi} + mgd_g\phi = qSbC_{l\delta_a}\delta_a + \tau + \frac{qSb}{V}C_{l\beta}W_y \tag{6}$$

where it is assumed that the rolling moment of the keel τ is known, and W_y models an unknown disturbance due to unknown gusts of lateral wind. The equation may be rewritten as

$$\ddot{\phi} + a_{\dot{\phi}}\dot{\phi} + a_\phi\phi = b_{\delta_a}\delta_a + \tau_{\text{keel}}/I_{xx} + b_{W_y}W_y/V$$

where in practice, the term $a_\phi\phi$ is small. There is a fast, stable, open-loop pole at $a_{\dot{\phi}} = p_0 = qSb^2C_{lp}/I_{xx}V \approx 40$ rad/s due to roll damping. The controller

$$\begin{aligned}\delta_a = \frac{1}{b_{\delta_a}}(&-p_1\dot{\phi} - p_0p_1\phi + a_\phi\phi + \ddot{\phi}_m \\ &+ (p_0+p_1)\dot{\phi}_m + p_0p_1\phi_m - M_{\text{keel}}/I_{xx})\end{aligned} \tag{7}$$

yields

$$(s+p_0)(s+p_1)\tilde{\phi} = b_{W_y}\frac{W_y}{V}. \tag{8}$$

When $p_1 \ll p_0$, the controller exploits the natural fast damping p_0 and maintains an acceptably small control activity because the feedback term in $\dot{\phi}$ is small (*i.e.* multiplied by p_1, not p_0). Unlike the longitudinal controller, this is a gain-scheduling controller, as the pole p_0 depends on V and is *a priori* time varying.

The steady-state gain for the sensitivity transfer function $W_y/V \mapsto \tilde{\phi}$ is 9°, meaning that for a system traveling at $V = 3W$, a lateral gust of intensity W may perturb the roll by no more than 3°. As stated above, for this experiment roll control is an easier problem than height control.

C. Yaw control

Yaw is passively stable. In this study a damping term is added to manual rudder input $\delta_{r,d}$: $\delta_r = -k_r\dot{\psi} + \delta_{r,d}$.

D. Keel control

A controller for the surface-piercing keel was presented in details in [21]. Interestingly, at the scales of interest, inertial effects are negligible (so that the system is first order), and the dynamics is dominated by the keel flexibility. The dynamics in [21] was formulated with the hypothesis that the vehicle's attitude remains horizontal and the travel direction constant. If the roll degree-of-freedom is also taken into account, the dynamics of the force generated by the keel (more precisely: its rolling moment τ) takes the form

$$(a_{\dot{\phi}}(t)/k)\dot{\tau} + \tau = b_\theta(t)\theta_k - a_{\dot{\phi}}(t)\dot{\phi} \tag{9}$$

where $a_{\dot{\phi}}$ and b_θ are possibly fast-varying parameters that depend on U and immersion depth h, as was described in [21]. Parameter k is the torsional spring constant that models the structural compliance of the keel under load. Parameters $a_{\dot{\phi}}$ and b_θ are related to the damping and lifting effect of the hydrodynamic forces, respectively. Like the aerodynamic coefficients, they can be modeled with AVL as detailed in [21].

Here again a feedback linearization controller

$$\theta_k = \frac{1}{b_\theta}\left(a_{\dot{\phi}}\dot{\phi} + \tau + \frac{a_{\dot{\phi}}(t)}{k}\left(-\lambda_{i,\tau}\tau + \dot{T}_d - \lambda_\tau\tilde{T}\right)\right)$$

is such that the error $\tilde{T} = T - T_d$ of the composite signal $T = \tau + \lambda_{i,\tau}\int\tau$ follows $(s+\lambda_\tau)T = 0$ which implies $\tau \to \tau_d$, where τ_d is the desired keel torque due to lift.

VI. Experiment

A. Experimental setup

The testing platform is composed of a Supra airframe fitted with a 2 cm-chord hydrofoil keel actuated in pitch and equipped with force sensing, as illustrated in figure 5. The keel subsystem was presented in details in [21]. The attitude and ground velocity of the system is estimated with an off-the-shelf estimator with the IMU of a Paparazzi Elle0 autopilot [22], [23]. The experiments were carried out in calm conditions where air-relative and ground-relative quantities are assumed to be equal. The load on the keel due to lift is measured with strain gauges positioned directly onto the hydrofoil shaft (figure 5). Finally, height above water and hydrofoil immersion are estimated with a Kalman filter that incorporates accelerometer, pressure and GPS measurements, as well as a downward-facing ultrasonic rangefinder attached to the airframe (figure 5 and [21]).

The maneuver of figure 4 was accomplished by towing the system at a constant or slowly-varying speed (7–10 m/s) on

the Charles River basin by means of a whaler boat (figure 5). The airframe was connected by its center of gravity to the tip of a fishing rod ahead of the boat. As described in figure 6, the airframe was connected to the towing whaler boat by three lines: towing line 1, remains taut at all times; safety lines 2 and 3 restrain the airframe when the experiment is not running. When the boat is still and no aerodynamic lift is generated by the airframe, the system is hanging from line 2. When the experiment is running, line 2 and 3 are slack and the system needs to be self-reliant for height control.

The inner-loop controllers discussed in the previous section were implemented on the on-board autopilot by Euler integration at 512 Hz. The desired trajectory z_d, τ_d was commanded by an operator by means of an RC transmitter.

B. Flight sequence

The typical experiment would proceed as follows: **0a**) The system starts from rest. The airframe is hanging from line 2 approximately 1 m above the water. **0b**) At rest, the autopilot is activated, which does not have any effect since the system is not moving. A height set-point of approximately 1.5 m is set. **0c**) The whaler boat accelerates until reaching 7–10 m/s. As stall speed is passed, the system autonomously "takes off" and reaches the set-point height, slacking safety line 2. **1**) Safety lines 2 and 3 are given full slack. The system is in flight, autonomously trailing at height z_d the attachment point of the towing line. **2**) The operator gives a down command to the system until z_d reaches the desired value for keel operation. The systems autonomously follows z_d and the keel enters the water. **3**) The operator gives a keel command τ_d away from the towing boat. The system autonomously generates the desired force with the keel, while maintaining its attitude and height above water. Because of the side force, the airframe is pushed sideways away from the boat. As a result the angle of the towing line changes (figure 6) and the towing force direction is shifted sideways. The system progresses sideways up to an equilibrium point where the side forces of the keel and towing line compensate each other. **4a**) The desired keel loading τ_d is brought back to 0, the desired height z_d is set back to a large value. The aircraft takes off and autonomously returns to trailing the towing line attachment point. **4b**) The safety lines are tightened, and the towing boat slows down to a rest.

VII. Experimental Results

The accompanying video, and figures 7 and 8 report a recording of the flight sequence described in section VI-B. The system is towed at 7 m/s. The sequence displayed starts in phase 1, and lasts for about 5 s while the system descends from 0.8 m to 0.3 m following the desired z_d trajectory input by the operator. At $t = 936$ s, the keel enters the water. The operator then sends a non-zero loading command to the keel, which is followed (albeit with some oscillation). Over a time span of approximately 20 seconds (140 m in distance), the keel generates on average the desired force, the height is controlled with centimeter accuracy (there is a small offset perhaps due to the unmodeled ground effect in equation (2), a small upwards force from the towing line whose attachment point is slightly higher than the aircraft, and our choice $\lambda_{i,z} = 0$ in the control law). Despite the oscillations of the keel forcing, pitch and roll are controlled within 2° from their desired value throughout the keel immersion event. Note that visual recordings of the experiment suggest a somewhat larger roll amplitude. This might be due to unmodeled flexibility of the wings and aircraft structure.

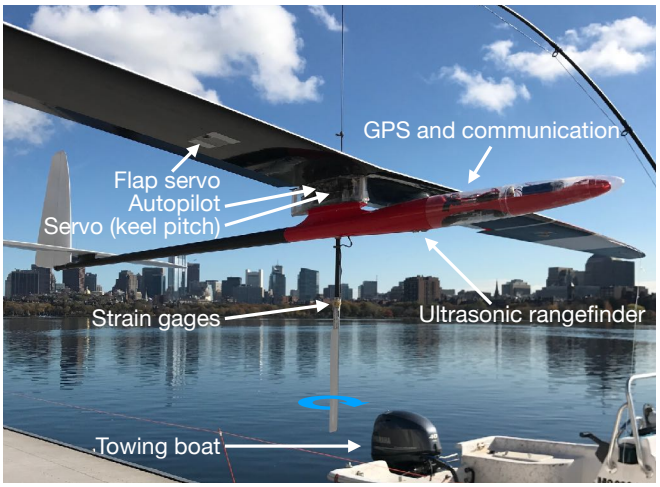

Fig. 5: Experimental setup: platform.

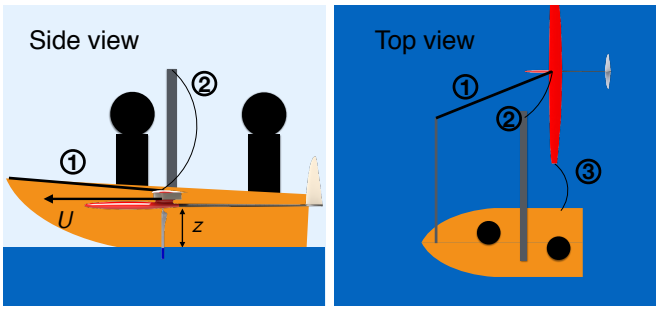

Fig. 6: Operations of the critical maneuver demonstration experiment.

VIII. Conclusions

In this study we introduced the UNAv, which borrows features from albatrosses and sailboats. It is designed to fly near the air-water interface, while being propelled by a sail and a surface-piercing keel. Trim calculations suggest that such a system could travel several times faster than traditional sailboats, require several times less wind than albatrosses to stay airborne, and have the ability to travel both upwind and downwind. A multi-input elevator+flaps longitudinal controller was developed for extreme low height flight. The combined feasibility of low height flight, keel immersion and keel force generation was demonstrated experimentally.

Finally, a UNAv operating dynamically in cycles of keel immersion and retraction, rather than in trim state, and generating the same average keel lift but in "bursts" of higher C_L would benefit from a higher average lift-to-drag ratio. Accordingly, the performance of UNAvs may be higher than that of the trim state operation presented in this study.

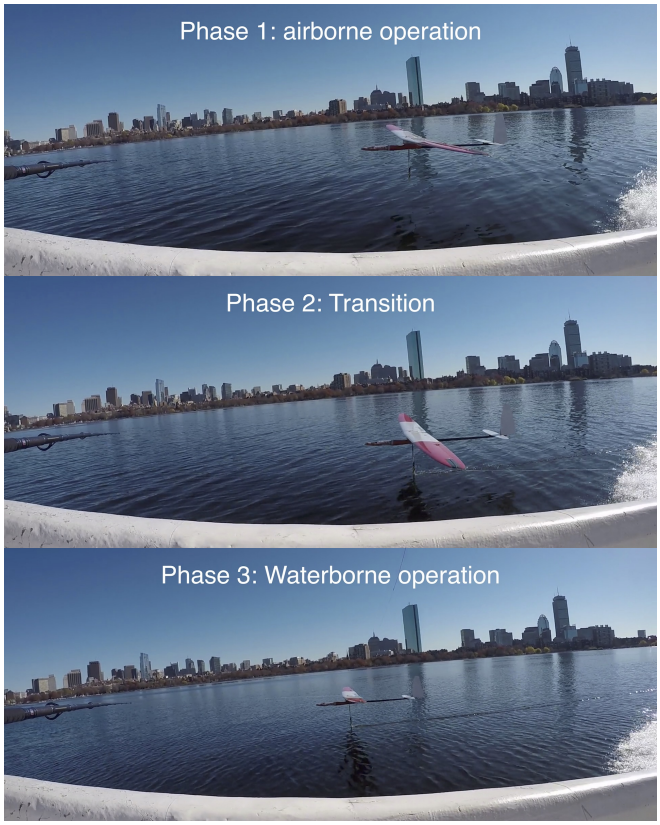

Fig. 7: Time-lapse of the critical maneuver demonstration. After phase 2, a side force is generated by the keel. It moves the aircraft away from the towing boat in phase 3.

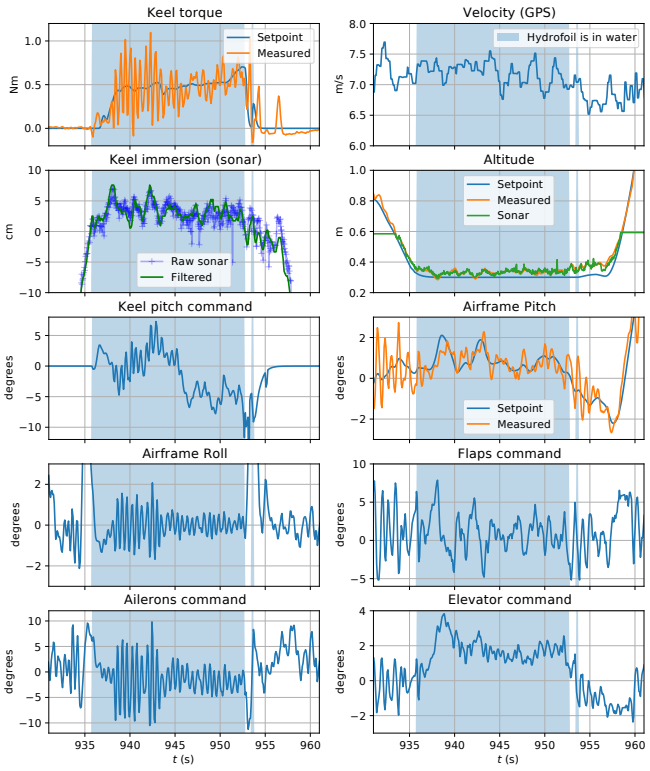

Fig. 8: Recording of the experiment of figure 7.

Acknowledgements

The paper is adapted from G.B.'s PhD thesis, with permission. We thank Michael Novitzky, Hugh Dougherty and Michael Benjamin from the LAMSS, as well as Stewart Craig from the MIT Sailing Pavilion for their help with the experiments. We thank Mark Drela and the members of the MIT Tow Tank lab for stimulating discussions. The paper is dedicated to Vanu Bose.

References

[1] P. Landschützer, N. Gruber *et al.*, "The reinvigoration of the Southern Ocean carbon sink," *Science*, vol. 349, no. 6253, pp. 1221–1224, 2015.

[2] M. J. Burton and W. W. Hoburg, "Solar-Electric and Gas Powered, Long-Endurance UAV Sizing via Geometric Programming," in *18th AIAA/ISSMO Multidisciplinary Analysis and Optimization Conference*, 2017.

[3] J. P. Nalepka and J. L. Hinchman, "Automated Aerial Refueling: Extending the Effectiveness of Unmanned Air Vehicles," in *AIAA Modeling and Simulation Technologies Conference and Exhibit*, San Francisco, CA, 2005, pp. 1–8.

[4] A. Noth, "Design of Solar Powered Airplanes for Continuous Flight," Ph.D. dissertation, ETH Zürich, 2008.

[5] P. Oettershagen, A. Melzer *et al.*, "A solar-powered hand-launchable UAV for low-altitude multi-day continuous flight," in *IEEE International Conference on Robotics and Automation (ICRA)*, Seattle, WA, 2015.

[6] C. C. Eriksen, T. J. Osse *et al.*, "Seaglider: A long-range autonomous underwater vehicle for oceanographic research," *IEEE Journal of Oceanic Engineering*, vol. 26, no. 4, pp. 424–436, 2001.

[7] J. Manley and S. Willcox, "The wave glider: A persistent platform for ocean science," in *OCEANS*, Sidney, Australia, 2010.

[8] C. Meinig, N. Lawrence-Slavas *et al.*, "The Use of Saildrones to Examine Spring Conditions in the Bering Sea: Vehicle Specification and Mission Performance," in *OCEANS*, Washington, DC, 2015.

[9] G. D. Bousquet, M. S. Triantafyllou, and J.-J. E. Slotine, "Optimal dynamic soaring consists of successive shallow arcs," *Journal of the Royal Society Interface*, vol. 14, no. 20170496, 2017.

[10] G. Sachs, J. Traugott *et al.*, "Flying at No Mechanical Energy Cost: Disclosing the secret of Wandering Albatrosses," *PLOS one*, vol. 7, no. 9, jan 2012.

[11] M. Drela and H. Youngren, "AVL (Athena Vortex Lattice)," 2007.

[12] M. Drela, *XFOIL: An Analysis and Design System for Low Reynolds Number Airfoils*. Springer, Berlin, Heidelberg, 1989, pp. 1–12.

[13] M. Drela, *Flight Vehicle Aerodynamics*. MIT press, 2014.

[14] J. N. Newman, *Marine hydrodynamics*. MIT press, 1977.

[15] Y. L. Young, C. M. Harwood *et al.*, "Ventilation of Lifting Bodies: Review of the Physics and Discussion of Scaling Effects," *Applied Mechanics Reviews*, vol. 69, 2017.

[16] S. F. Hoerner, *Fluid-Dynamic Drag*. Published by the author, 1965.

[17] G. Bower, "Boundary Layer Dynamic Soaring for Autonomous Aircraft: Design and Validation," Ph.D. dissertation, Stanford University, 2011.

[18] H. Weimerskirch, T. Guionnet *et al.*, "Fast and fuel efficient? Optimal use of wind by flying albatrosses," *Philosophical Transactions: Biological Sciences*, vol. 267, pp. 1869–74, sep 2000.

[19] J.-J. E. Slotine and W. Lohmiller, "Modularity, evolution, and the binding problem: a view from stability theory," *Neural Networks*, vol. 14, pp. 137–145, 2001.

[20] W. Lohmiller and J.-J. E. Slotine, "On Contraction Analysis for Nonlinear Systems," *Automatica*, vol. 34, no. 6, pp. 683–696, 1999.

[21] G. D. Bousquet, M. S. Triantafyllou, and J.-J. E. Slotine, "Control of a flexible, surface-piercing hydrofoil for high-speed, small-scale applications," in *IEEE International Conference on Intelligent Robots and Systems (IROS)*, Vancouver, BC, Canada, 2017.

[22] P. Brisset, A. Drouin *et al.*, "The Paparazzi Solution," in *MAV 2006, 2nd US-European Competition and Workshop on Micro Air Vehicles*, 2006.

[23] G. Hattenberger, M. Bronz, and M. Gorraz, "Using the Paparazzi UAV System for Scientific Research," *IMAV 2014, International Micro Air Vehicle Conference and Competition 2014*, pp. 247–252, 2014.